Electronic Supplementary Material (ESI) for Dalton Transactions.
This journal is © The Royal Society of Chemistry 2020

Electronic Supplementary Information

Synthesis and structures of mono- and di-nuclear aluminium and zinc complexes bearing α-diimine and related ligands, and their use in the ring opening polymerization of cyclic esters

Lin Xiao,[a] Yanxia Zhao,[a*] Sijie Qiao,[a] Ziyue Sun,[a] Orlando Santoro[b] and Carl Redshaw[a,b*]

[a] *College of Chemistry and Material Science, Northwest University, 710069 Xi'an, China*
[b] *Department of Chemistry & Biochemistry, The University of Hull, Cottingham Rd, Hull, HU6 7RX, U.K.*

Contents

Figure S29. 2D J-resolved ^{1}H NMR ($CDCl_3$, 400 MHz, 298 K) spectrum of the PLA synthesized with **6** at 80 ºC (Table 6, entry 2).

Figure S30. 2D J-resolved ^{1}H NMR ($CDCl_3$, 400 MHz, 298 K) spectrum of the PLA synthesized with **7** at 30 ºC (Table 6, entry 3).

Figure S31. 2D J-resolved ^{1}H NMR ($CDCl_3$, 400 MHz, 298 K) spectrum of the PLA synthesized with **7** at 80 ºC (Table 6, entry 4).

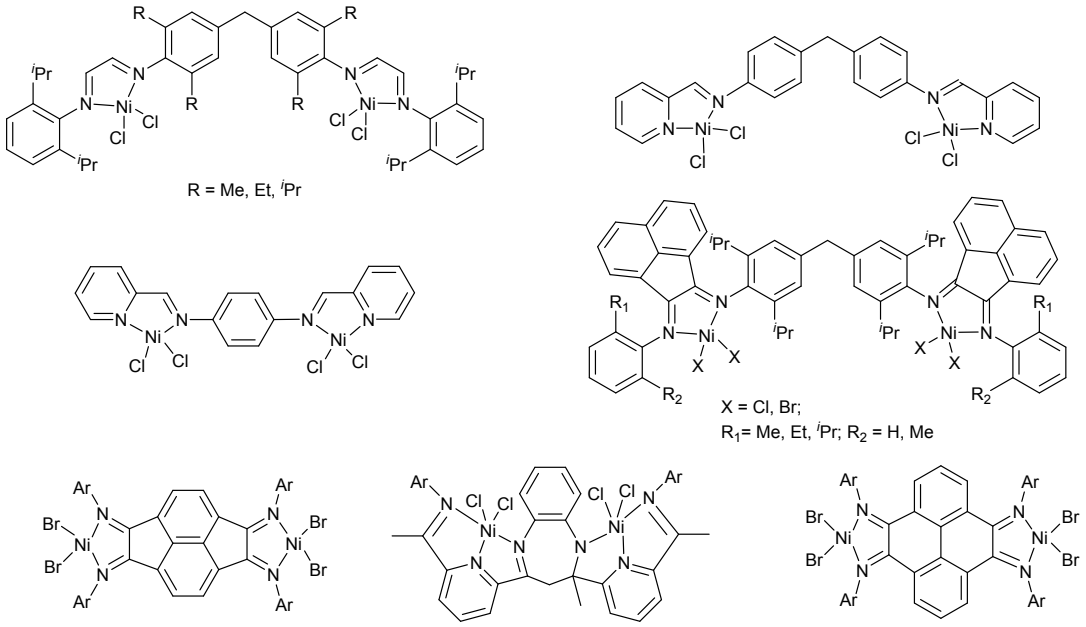

Chart S1. Imine-based frameworks utilized in bi-nickel-based olefin polymerization chemistry. [1]

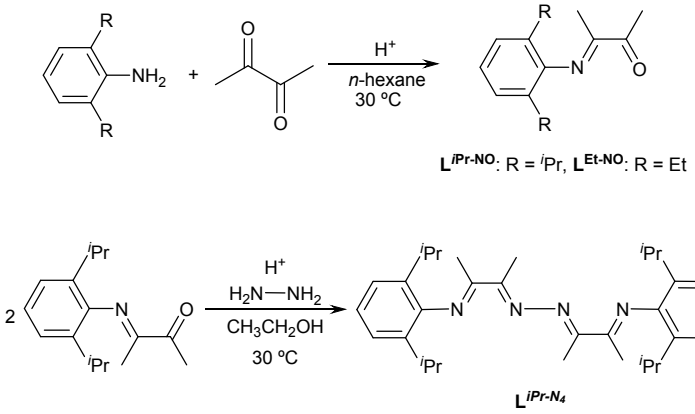

Scheme S1. Synthesis of the ligands $\mathbf{L}^{i\mathbf{Pr\text{-}NO}}$, $\mathbf{L}^{\mathbf{Et\text{-}NO}}$ and $\mathbf{L}^{\mathbf{ipr\text{-}N4}}$.

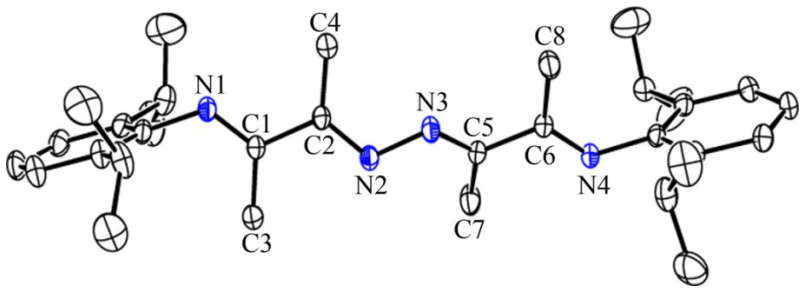

Figure S1. The molecular structure of $\mathbf{L}^{i\mathbf{Pr\text{-}N_4}}$ (thermal ellipsoids are set at the 20% probability level; H atoms are omitted for clarity): C1–N1 1.269(3), C1–C2 1.498(3), C1–C3 1.497(4), C2–N2 1.277(3), C2–C4 1.483(4), N2–N3 1.405(3), C5–N3 1.279(3), C5–C7 1.479(4), C5–C6 1.496(3), C6–N4 1.274(3), C6–C8 1.496(4); N1–C1–C2 116.0(2), C1–C2–N2 115.6(2), C2–N2–N3 115.2(2), N2-C3-N5 114.7(2), N3–C5–C6 115.6(2), C5–C6–N4 116.2(2).

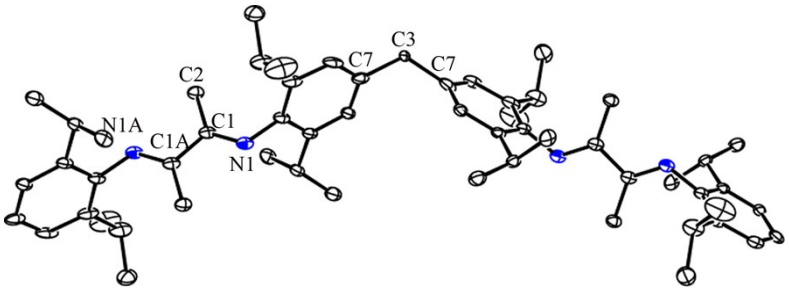

Figure S2. The molecular structure of $\mathbf{L}^{i\mathbf{Pr}\text{-}\mathbf{N_2}\text{-}\mathbf{ArCH_2Ar}\text{-}\mathbf{N_2}}$ (thermal ellipsoids are set at the 20% probability level; H atoms are omitted for clarity): C1–N1 1.291(4), C1–C2 1.505(4), C1–C1A 1.518(4), N1–C1–C2 126.5(3), N1–C1–C1 116.4(4), C2–C1–C1 117.1(4),C7–C3–C7 121.7(5).

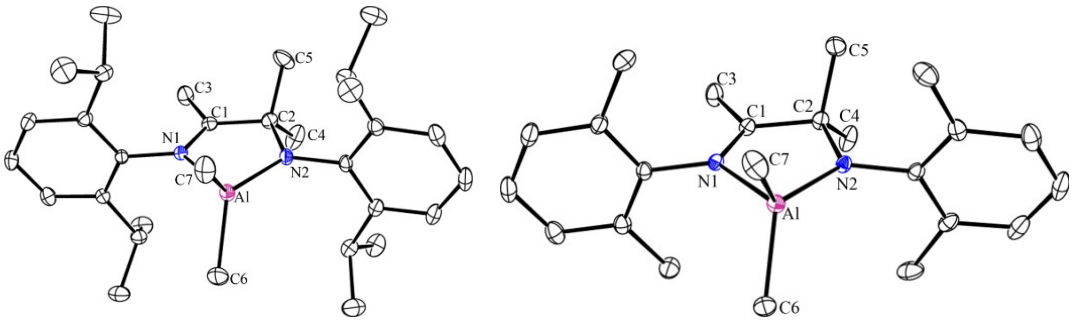

Figure S3. The molecular structure of **1** (left), **3** (right) (thermal ellipsoids are set at the 20% probability level; H atoms are omitted for clarity).

Theoretical Calculations

Structure optimization for the model compounds $[ArN{-}C(Me)_2C(Me){=}NAlMe_2]_2$ (**4**) and its isomers **4a** and **4b**, were carried out at the DFT (B3LYP) level with a 6-31G*[2,3] basis set using the Gaussian 09 program.[4] Figure S4 shows the optimized geometries. Here DFT results show that **4** exhibits a slightly lower energy than the imino-amido isomer **4a** (ΔE = 18.0 kJ mol^{-1}) and **4b** (30.3 kJ mol^{-1}).

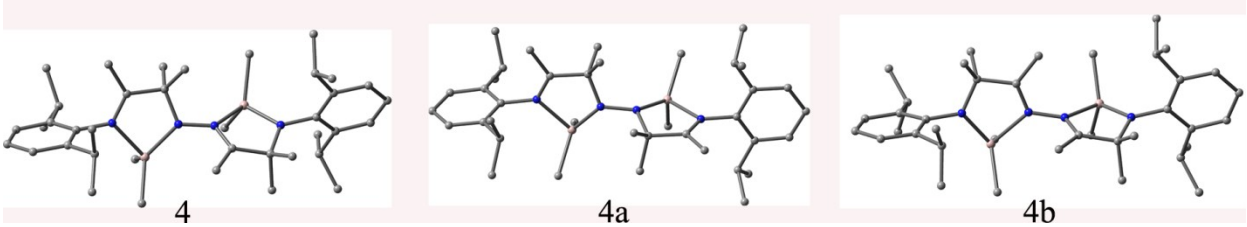

Figure S4. Optimized structures of **4** and its isomers **4a** and **4b**.

Table S1. Relative energies of compounds **4 and** , **4a** and **4b**.

Compound	Energy (E, a.u.)	ΔE (kJ/mol)
4	–2190.58568031	0
4a	–2190.57882952	18.0
4b	–2190.57413253	30.3

Table S2. Crystallographic data and refinement details for compounds $\mathbf{L}^{i\mathbf{Pr\text{-}N4}}$, **1**–**3**.

Compound	$\mathbf{L}^{i\mathbf{Pr\text{-}N4}}$	**1**	**2**	**3**
Empirical formula	$C_{32}H_{46}N_4$	$C_{31}H_{49}AlN_2$	$C_{27}H_{41}AlN_2$	$2*C_{23}H_{33}AlN_2$
Fw	486.73	476.70	420.60	728.98
Crystal system	Triclinic	Triclinic	monoclinic	monoclinic
Space group	$P\bar{1}$	$P\bar{1}$	Cc	$P2_1/c$
a /Å	10.030(4)	8.4984(18)	9.425(2)	14.239(13)
b /Å	12.557(4)	9.799(2)	37.074(9)	8.148(3)
c /Å	13.499(5)	19.426(4)	8.102(2)	38.13(2)
α /°	66.078(4)	82.115(3)	90	90
β /°	84.299(5)	80.860(2)	111.579(3)	91.22(3)
γ /°	82.021(5)	69.630(2)	90	90
V /Å^3	1537.3(9)	1491.4(5)	2632.9(11)	4423(5)
Z	2	2	4	4
D_{calc}/g cm^{-3}	1.051	1.062	1.061	1.095
F (000)	532	524	920	1584
μ /mm^{-1}	0.062	0.088	0.092	0.100
θ range	1.785−24.970	2.132−24.997	2.197−24.958	2.719−25.242
Reflns collected	9657	9538	8102	21974
Independent reflns	5712	5095	8102	7701
Reflns [$I>2\sigma(I)$]	3705	3943	7632	5035
R_{int}	0.0326	0.0255	0.0285	0.0705
R_1;wR_2 [$I>2\sigma(I)$]	0.0746; 0.1580	0.0608; 0.1741	0.0396; 0.1134	0.0589; 0.1038
R_1; wR_2 (all data)	0.0981; 0.1694	0.0782; 0.1873	0.0426; 0.1163	0.1043; 0.1256
GOF (F^2)	1.042	1.155	1.023	1.121

Table S3. Crystallographic data and refinement details for compounds **4–7**.

Compound	**4**	**5**	**6**	**7**·0.5toluene
Empirical formula	$C_{38}H_{64}Al_2N_4$	$C_{34}H_{56}Al_2N_2O_2$	$C_{32}H_{50}ZnN_2$	$C_{54}H_{83}Zn_3N_3O_3$• 0.5toluene
Fw	630.89	578.76	528.11	1064.49
Crystal system	Monoclinic	Monoclinic	monoclinic	Orthorhombic
Space group	P21/c	$P2_1/n$	$P2_1/c$	Pca21
a /Å	13.900(5)	8.505(3)	8.5697(19)	28.2584(16)
b /Å	18.370(6)	13.440(5)	19.226(4)	15.9307(9)
c /Å	16.078(6)	14.919(7)	18.509(4)	13.3344(6)
α /°	90	90	90	90
β /°	106.950(14)	94.584(13)	93.238(8)	90
γ /°	90	90	90	90
V /Å^3	3927(2)	1699.8(11)	3044.6(11)	6002.8(6)
Z	4	2	4	4
D_{calc}/g cm^{-3}	1.067	1.131	1.152	1.127
F (000)	1384	632	1144	2168
μ /mm^{-1}	0.103	0.116	0.827	1.227
θ range	1.727−24.997	2.669−25.342	2.388 − 26.364	2.459−26.389
Reflns collected	37227	18303	17326	39300
Independent reflns	6900	3091	6030	11494
Reflns [$I > 2\sigma(I)$]	5479	2722	322	9673
R_{int}	0.0720	0.0285	0.0351	0.0485
R_1;wR_2 [$I > 2\sigma(I)$]	0.0714; 0.2088	0.0330; 0.0731	0.0518; 0.1020	0.0399; 0.0749
R_1; wR_2 (all data)	0.0877; 0.2088	0.0394; 0.0770	0.0696; 0.1093	0.0527; 0.0796
GOF (F^2)	1.005	1.029	1.130	1.038

Table S4. Crystallographic data and refinement details for compounds $\mathbf{L}^{i\mathbf{Pr\text{-}N2\text{-}ArCH2Ar\text{-}N2}}$ and **8**.

Compound	$\mathbf{L}^{i\mathbf{Pr\text{-}N2\text{-}ArCH2Ar\text{-}N2}}$	**8**·3.5toluene
Empirical formula	$C_{57}H_{80}N_4$	$C_{57}H_{80}Cl_4N_4Zn_2$·3.5 toluene
Fw	821.25	1410.59
Crystal system	monoclinic	monoclinic
Space group	C2/c	P21/n
a /Å	16.4092(9)	13.65(3)
b /Å	9.5095(9)	25.08(5)
c /Å	17.0073(10)	24.33(5)
α /°	90	90
β /°	108.349(3)	92.47(7)
γ /°	90	90
V /Å^3	2518.9(3)	8319(31)
Z	2	4
D_{calc}/g cm^{-3}	1.083	0.873
F (000)	900	2312
μ /mm^{-1}	0.062	0.732
θ range	2.51–25.10	2.32−21.79
Reflns collected	10737	14853
Independent reflns	5944	9937
Reflns [$I > 2\sigma(I)$]	1603	7649
R_{int}	0.0463	0.0819
R_1;wR_2 [$I > 2\sigma(I)$]	0.0936; 0.1672	0.0740; 0.1906
R_1; wR_2 (all data)	0.1268; 0.1849	0.1308; 0.2107
GOF (F^2)	1.058	1.024

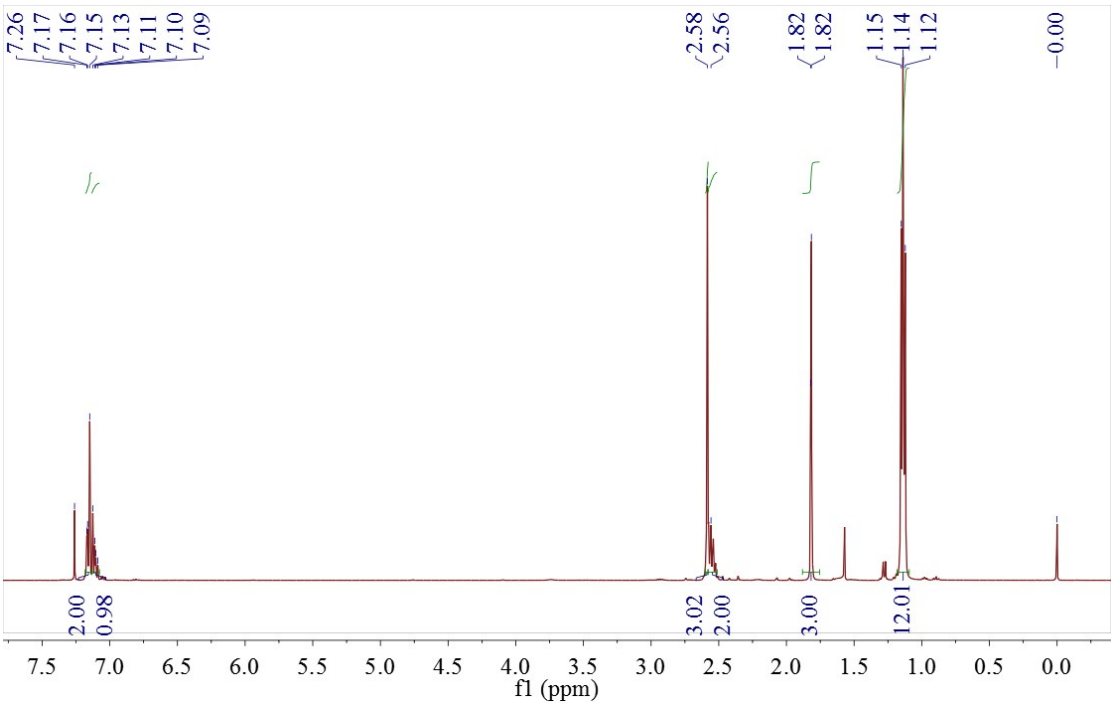

Figure S5. ^{1}H NMR (400 MHz $CDCl_3$ 298K) spectrum for ligand **L$^{i\text{Pr-NO}}$**.

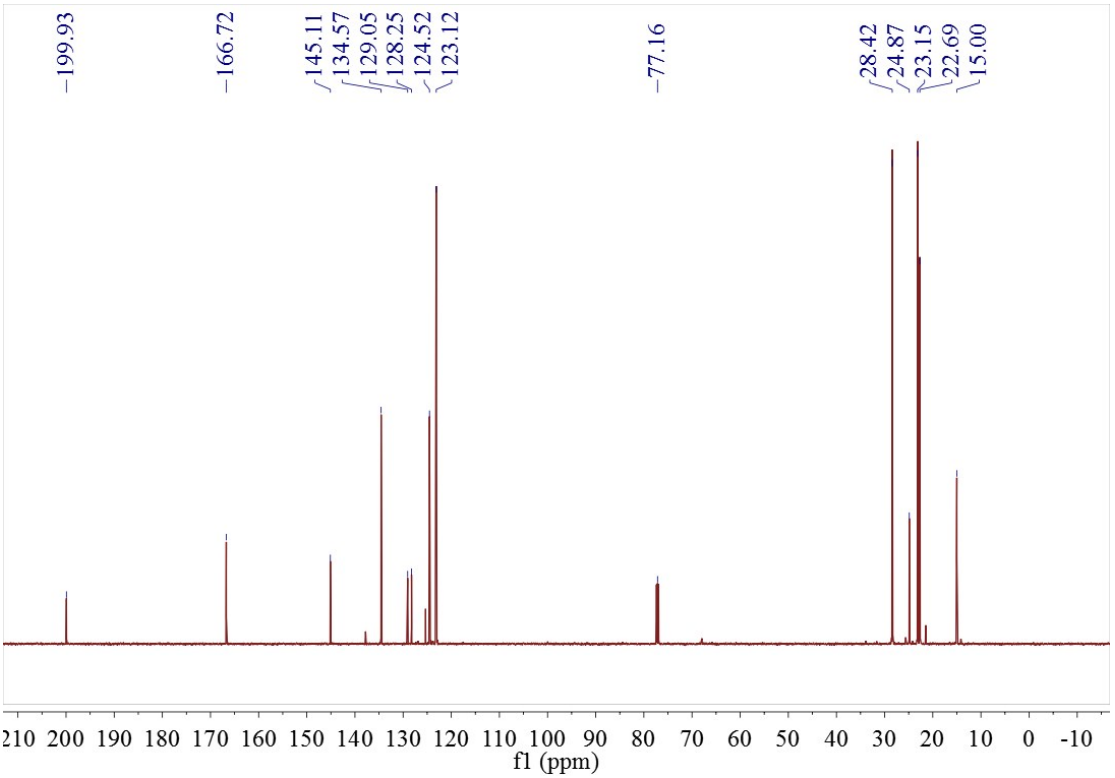

Figure S6. ^{13}C NMR (100.6 MHz $CDCl_3$ 298K) spectrum for ligand **L$^{i\text{Pr-NO}}$**.

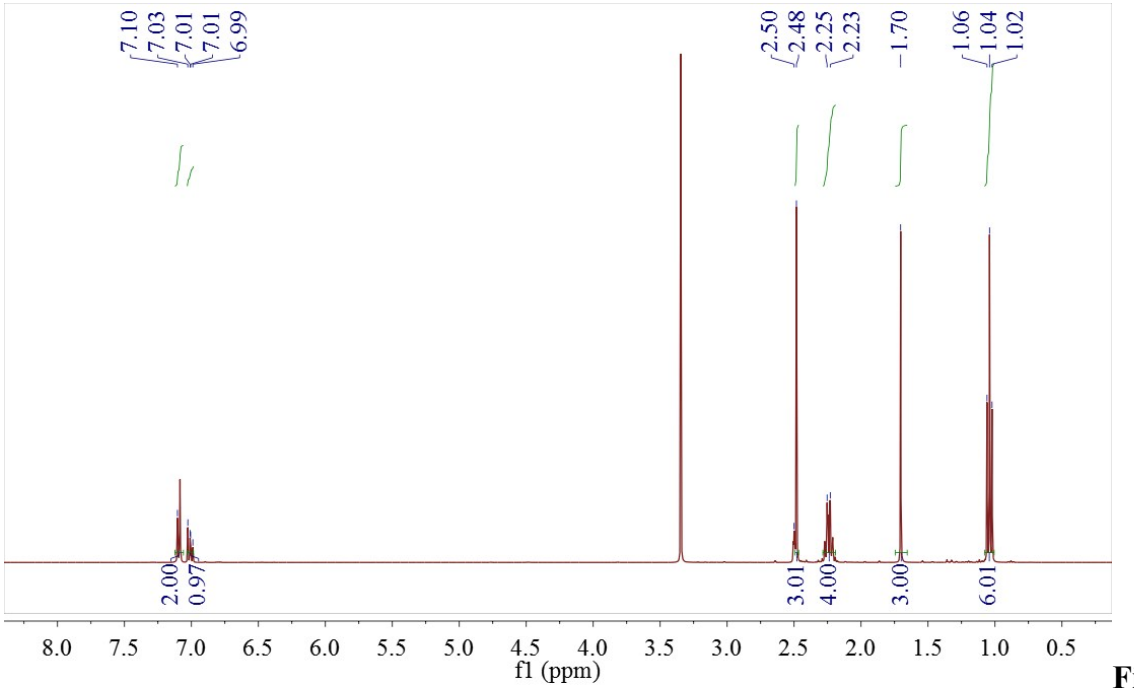

Figure S7. ^{1}H NMR (400 MHz DMSO 298K) spectrum for ligand $\mathbf{L^{Et\text{-}NO}}$.

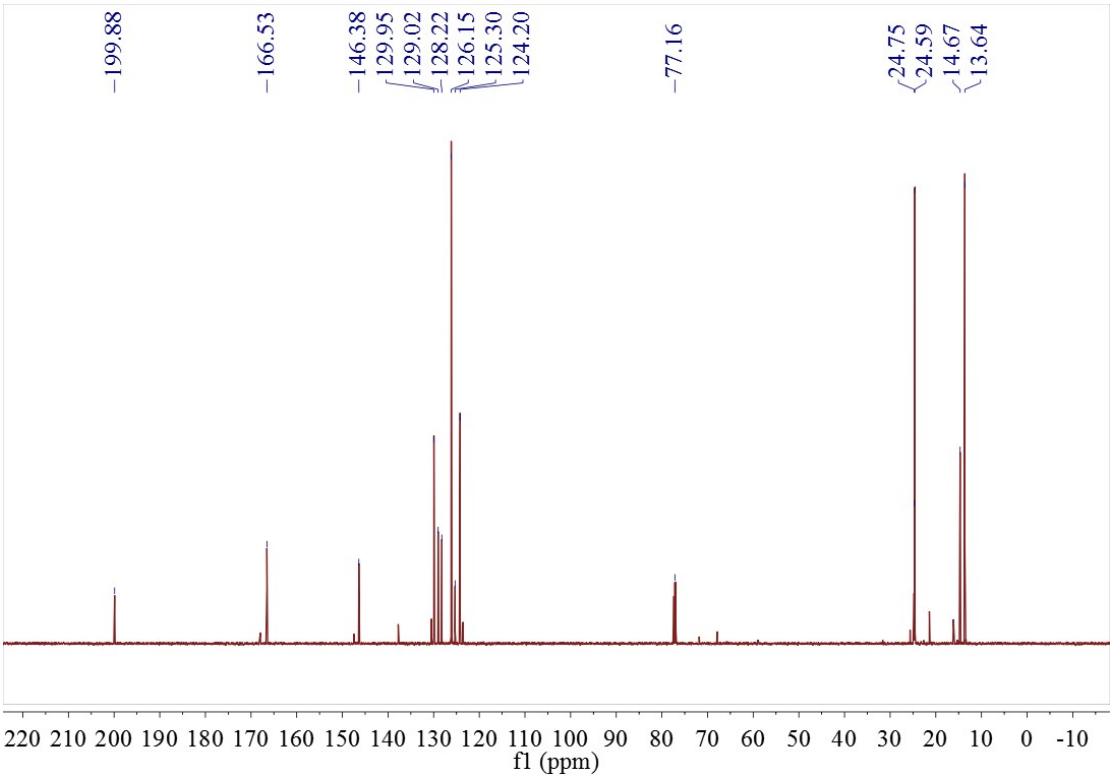

Figure S8. ^{13}C NMR (100.6 MHz $CDCl_3$ 298K) spectrum for ligand $\mathbf{L^{Et\text{-}NO}}$.

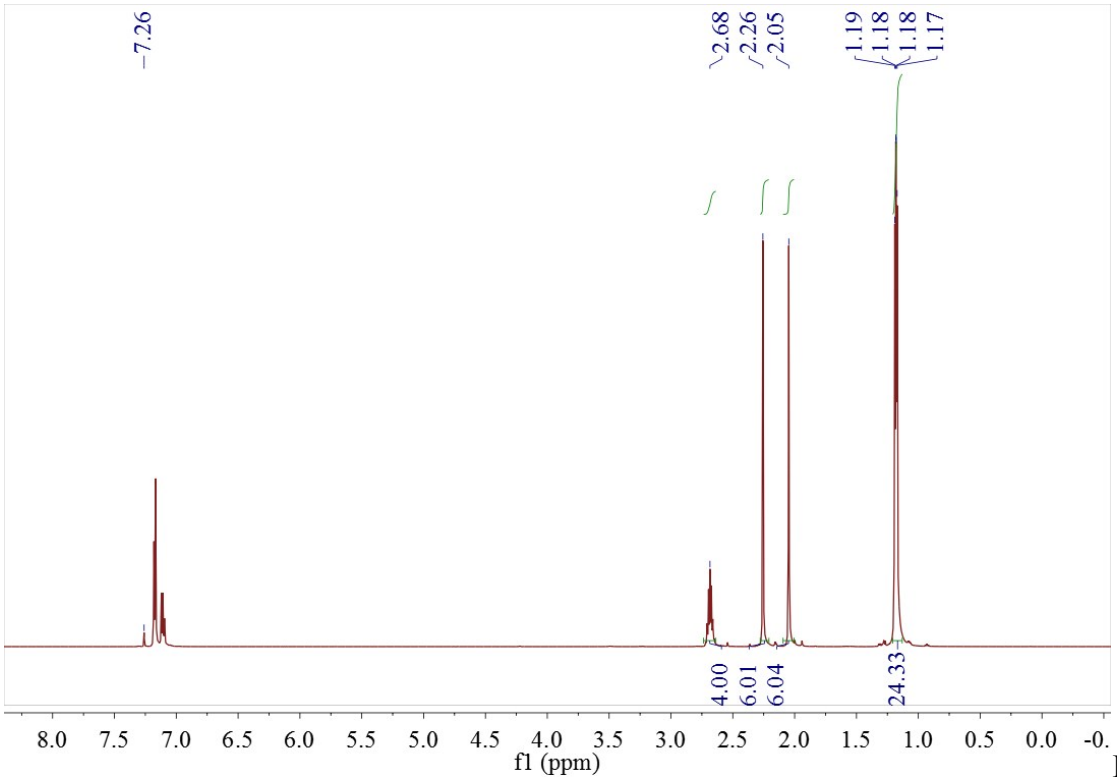

Figure S9. ^{1}H NMR (400 MHz $CDCl_3$ 298K) spectrum for ligand $\mathbf{L^{ipr\text{-}N4}}$.

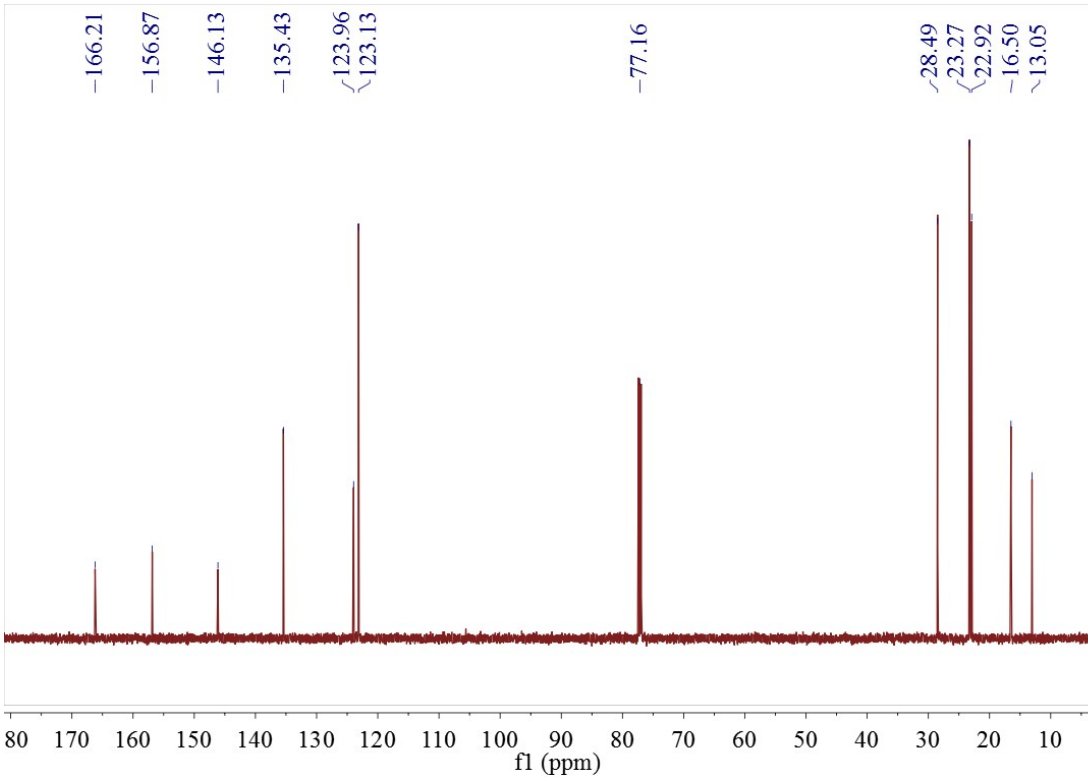

Figure S10. ^{13}C NMR (100.6 MHz $CDCl_3$ 298K) spectrum for ligand $\mathbf{L^{ipr\text{-}N4}}$.

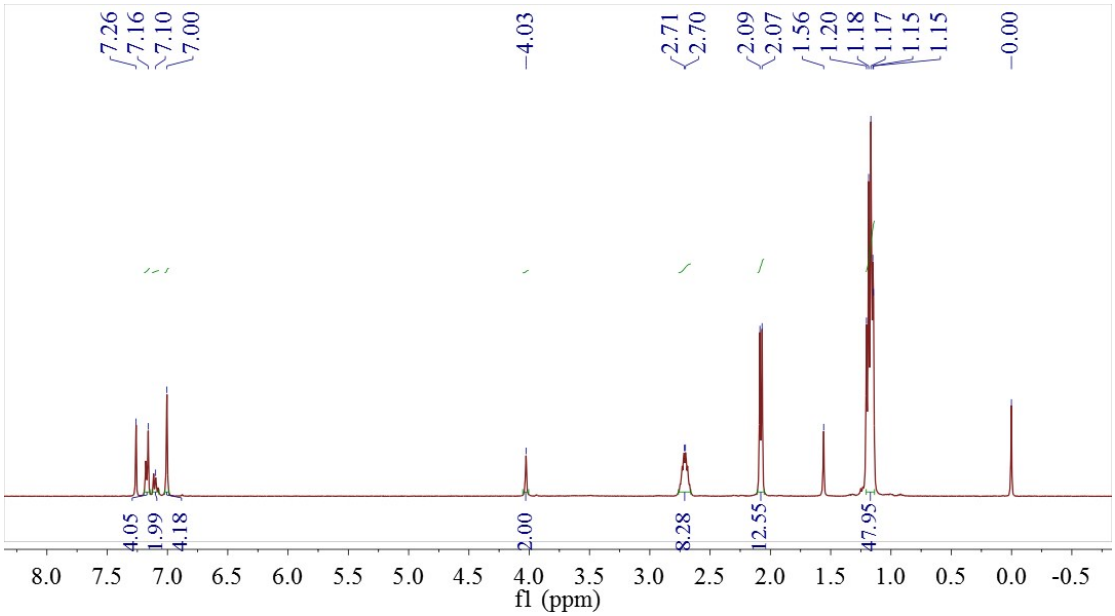

Figure S11. ^{13}H NMR (400 MHz $CDCl_3$ 298K) spectrum for ligand $\mathbf{L^{iPr\text{-}N2\text{-}ArCH2Ar\text{-}N2}}$

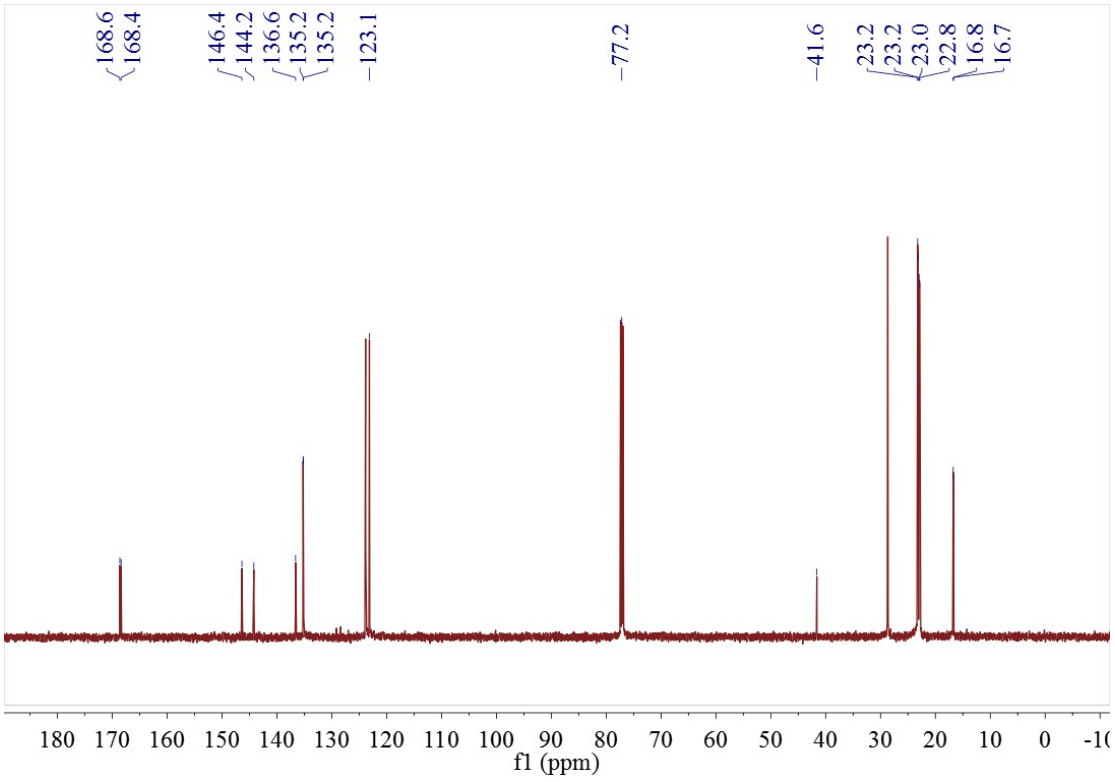

Figure S12. ^{13}C NMR (100.6 MHz $CDCl_3$ 298K) spectrum for ligand $\mathbf{L^{iPr\text{-}N2\text{-}ArCH2Ar\text{-}N2}}$

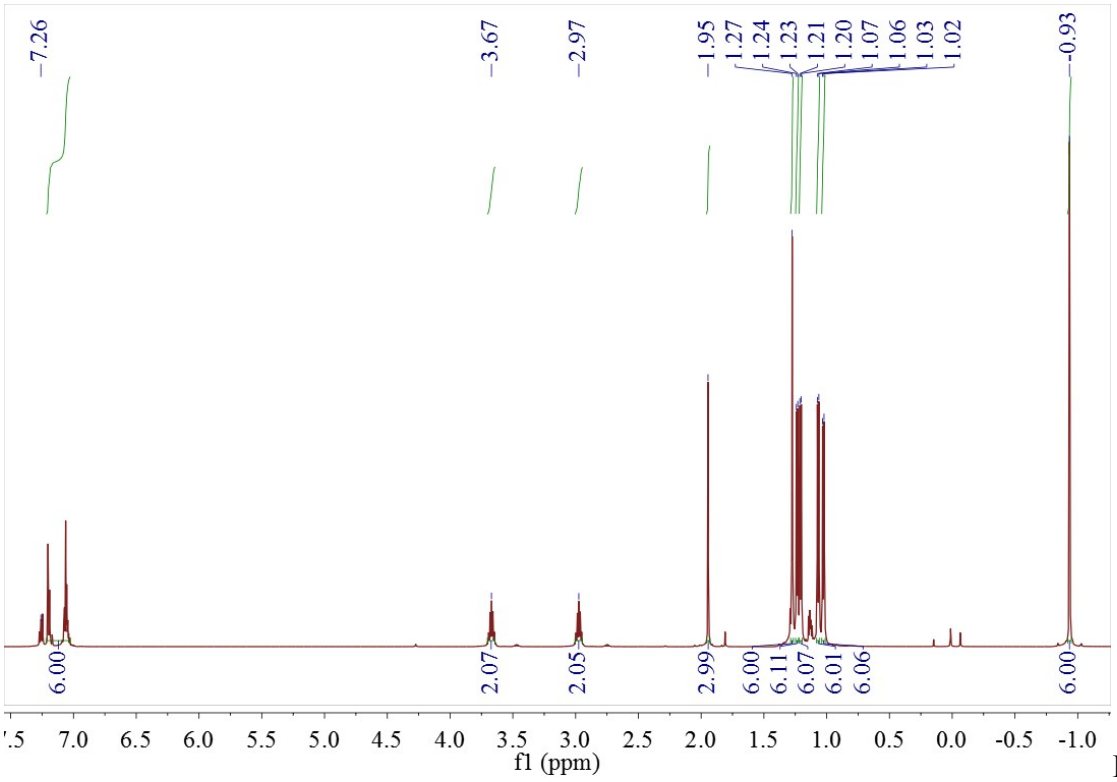

Figure S13. ^{1}H NMR (400 MHz $CDCl_3$ 298K) spectrum for compound **1.**

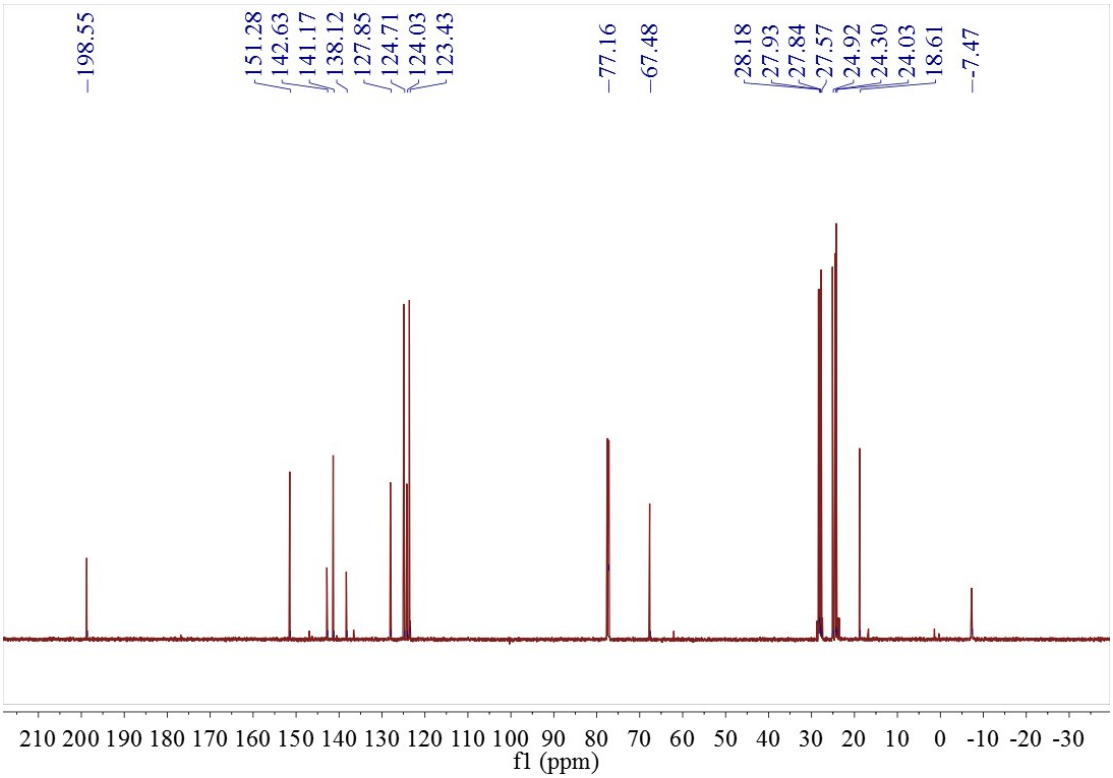

Figure S14. ^{13}C NMR (100.6 MHz $CDCl_3$ 298K) spectrum for compound **1**.

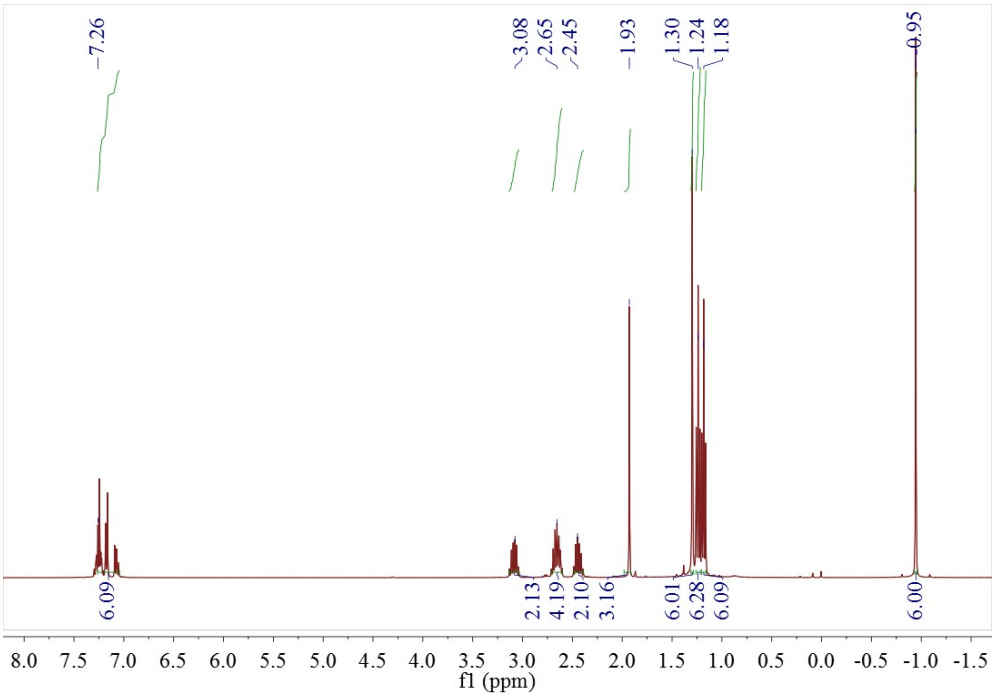

Figure S15. ^{1}H NMR (400 MHz $CDCl_3$ 298K) spectrum for compound **2**.

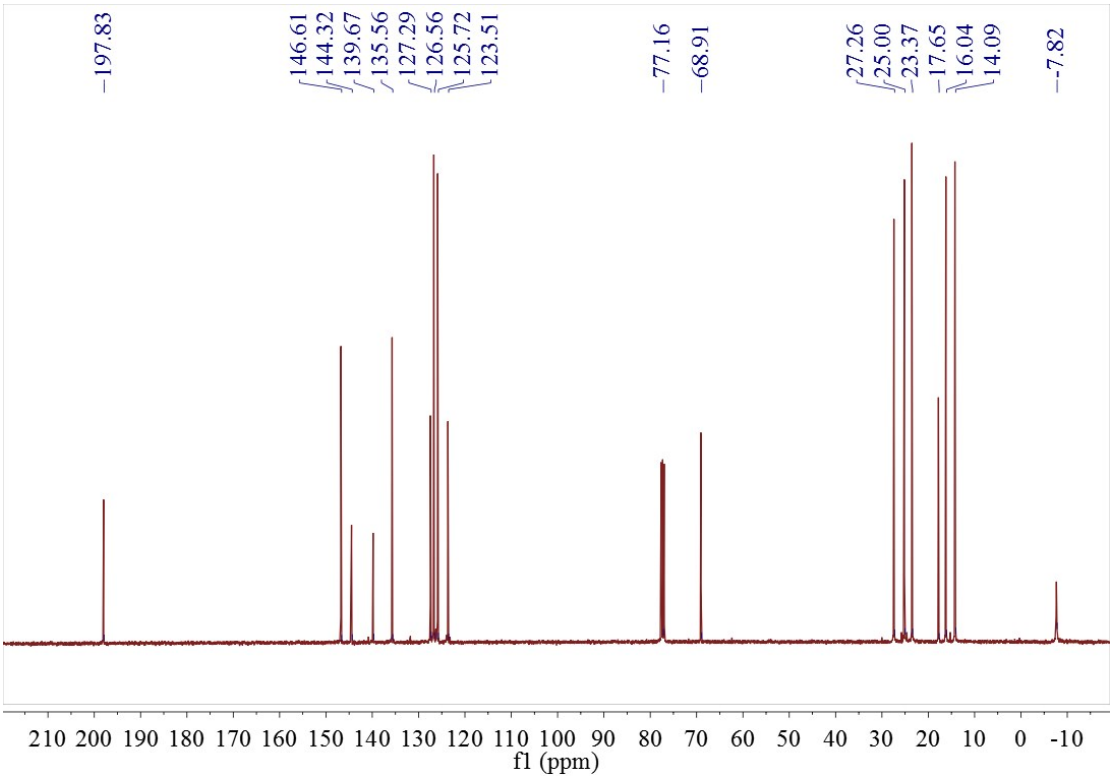

Figure S16. ^{13}C NMR (100.6 MHz $CDCl_3$ 298K) spectrum for compound **2**.

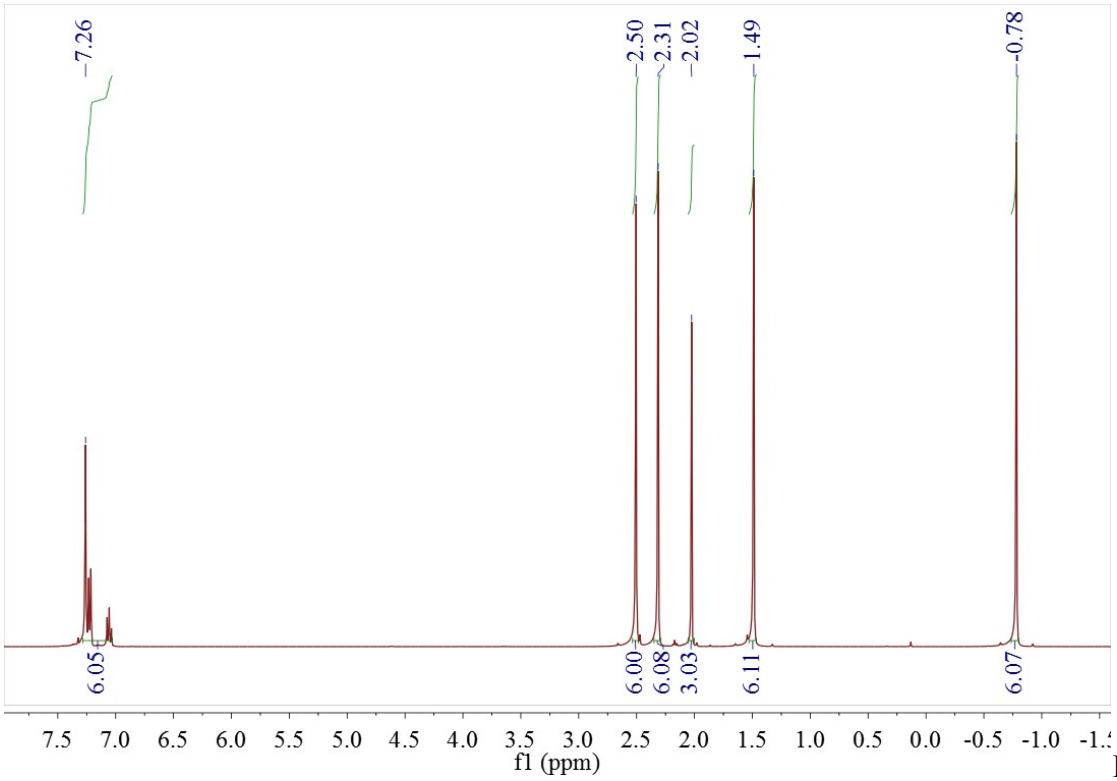

Figure S17. ^{1}H NMR (400 MHz $CDCl_3$ 298K) spectrum for compound **3**.

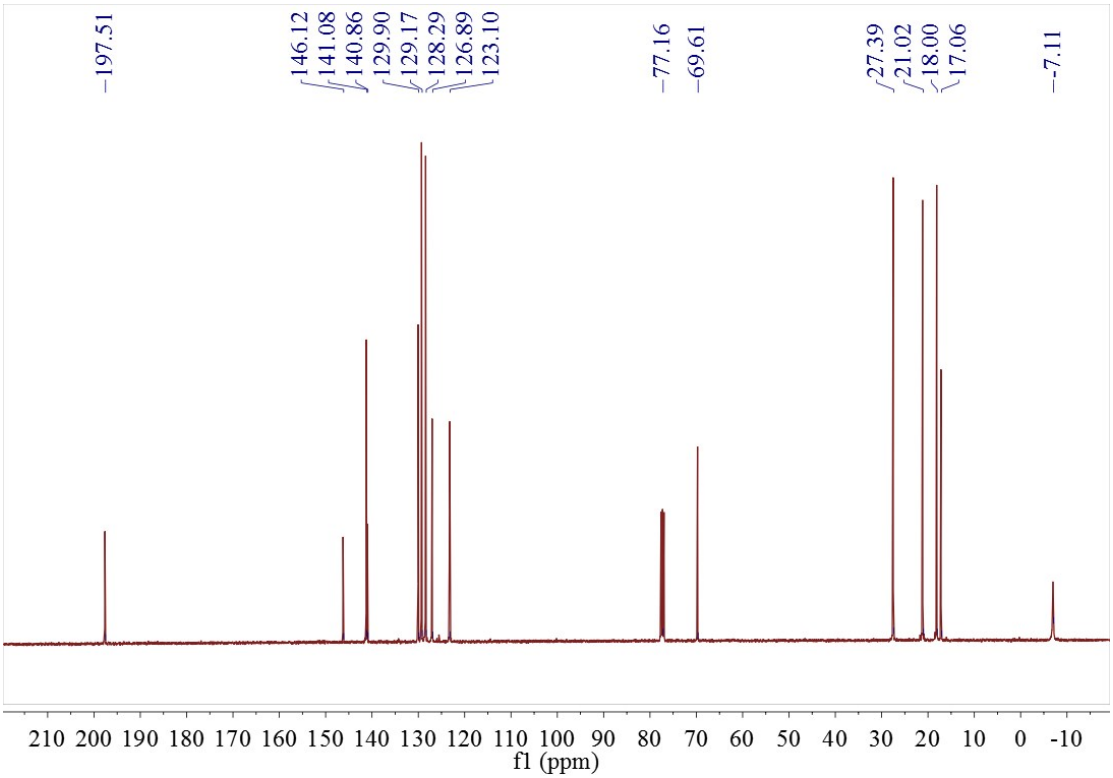

Figure S18. ^{13}C NMR (100.6 MHz $CDCl_3$ 298K) spectrum for compound **3**.

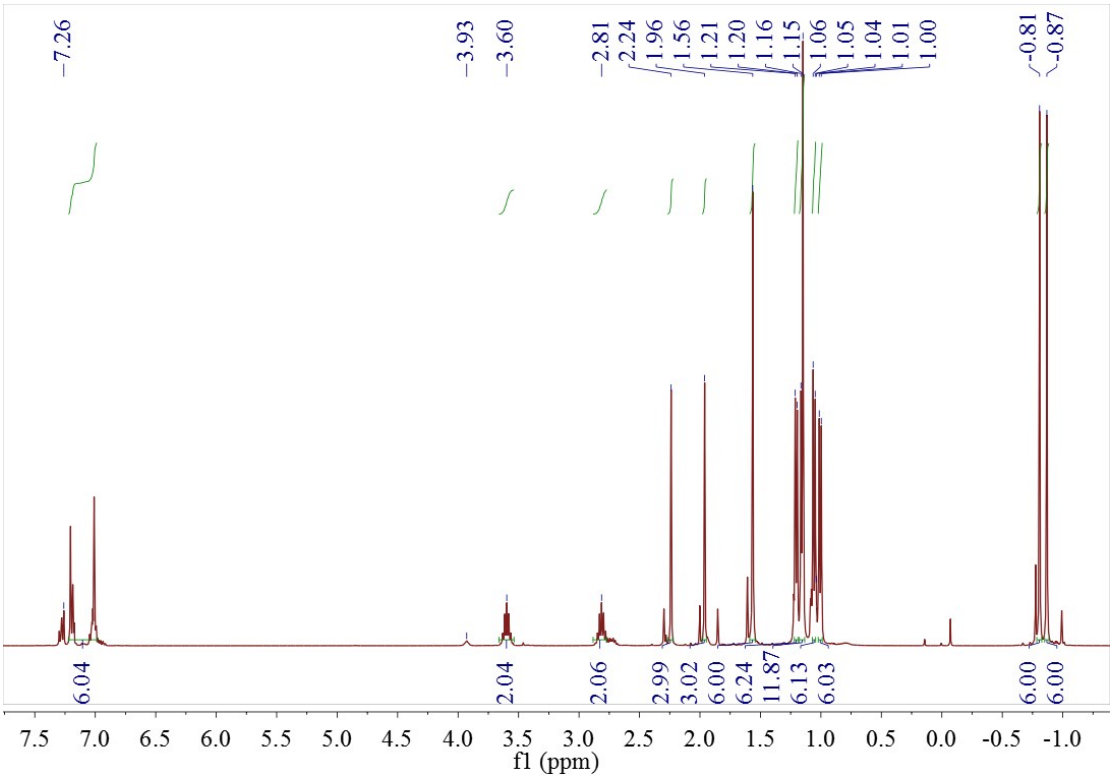

Figure S19. ^{1}H NMR (400 MHz $CDCl_3$ 298K) spectrum for compound **4**.

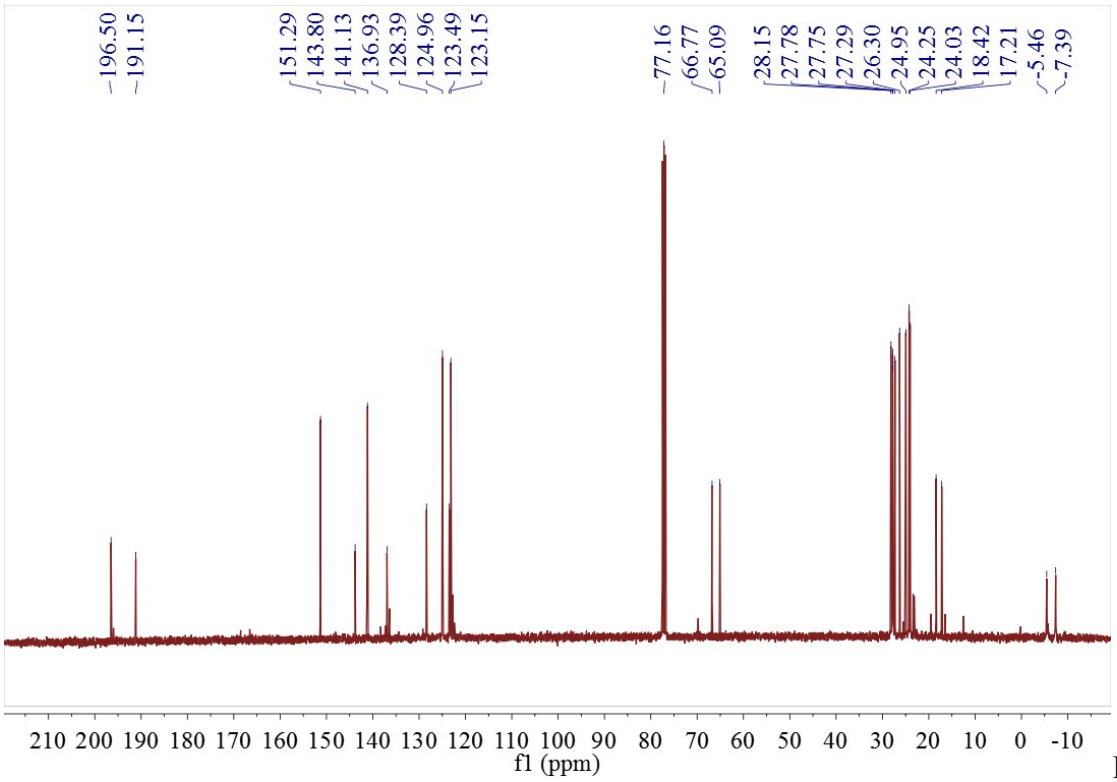

Figure S20. ^{13}C NMR (100.6 MHz $CDCl_3$ 298K) spectrum for compound **4**.

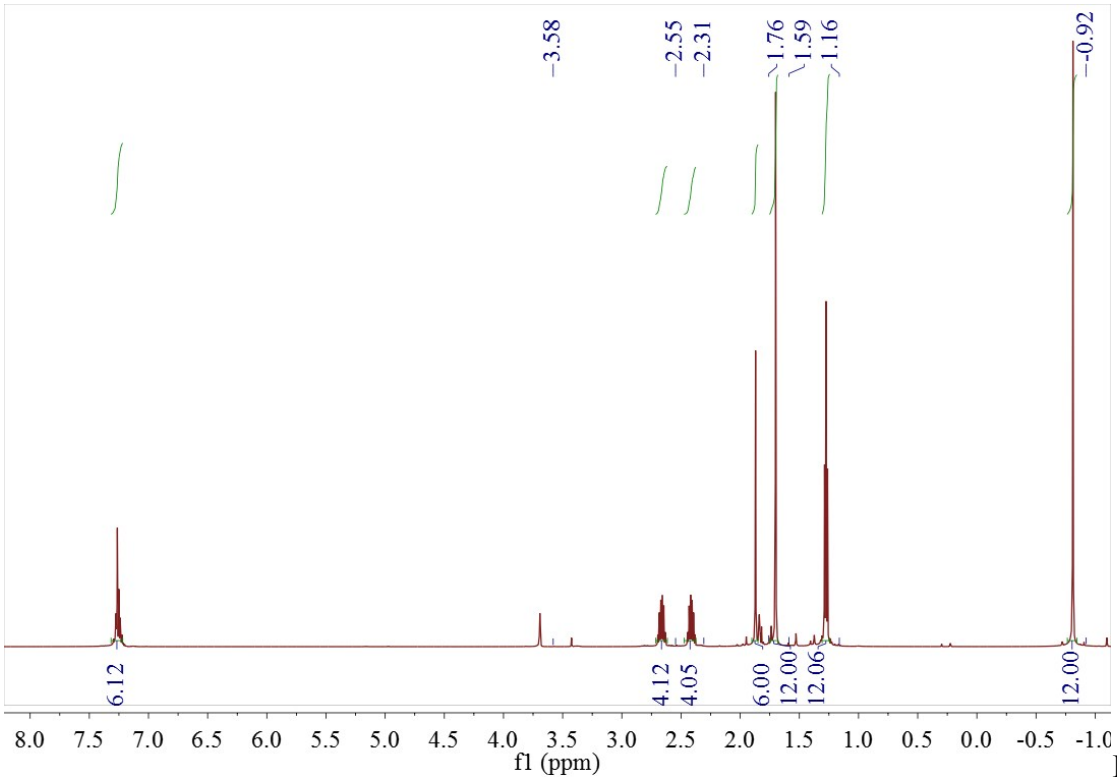

Figure S21. ^{1}H NMR (400 MHz THF-d8 298K) spectrum for compound **5**.

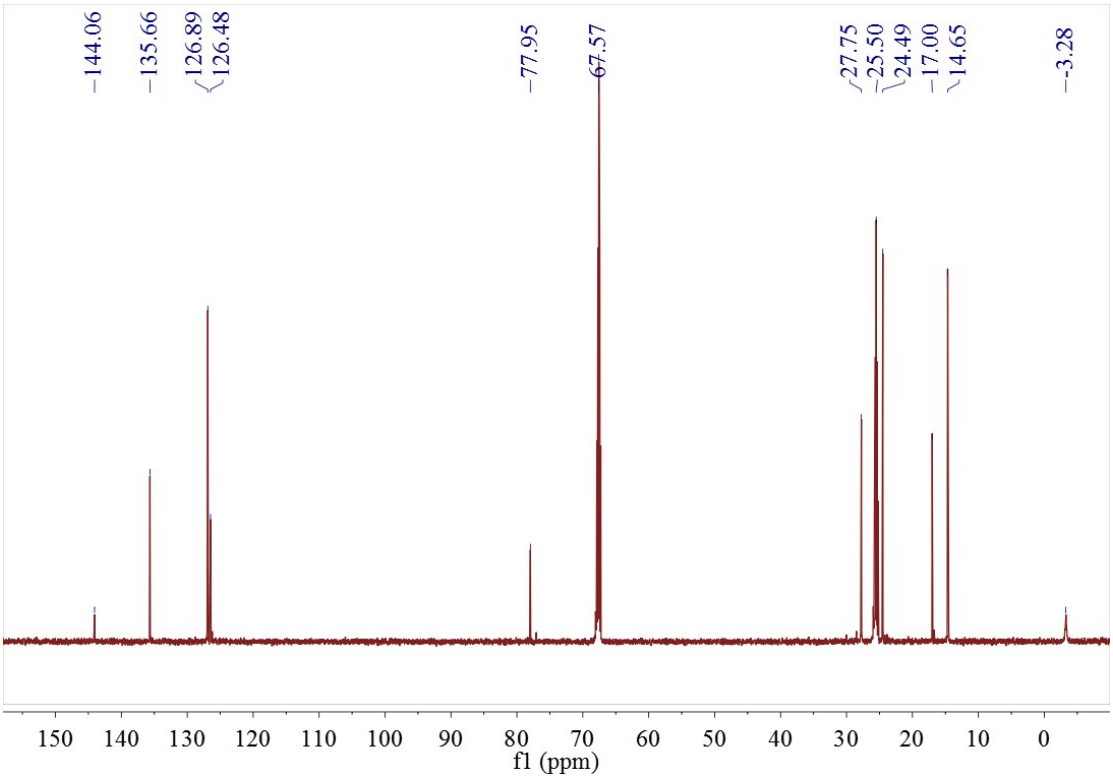

Figure S22. ^{13}C NMR (100.6 MHz THF-d8 298K) spectrum for compound **5**.

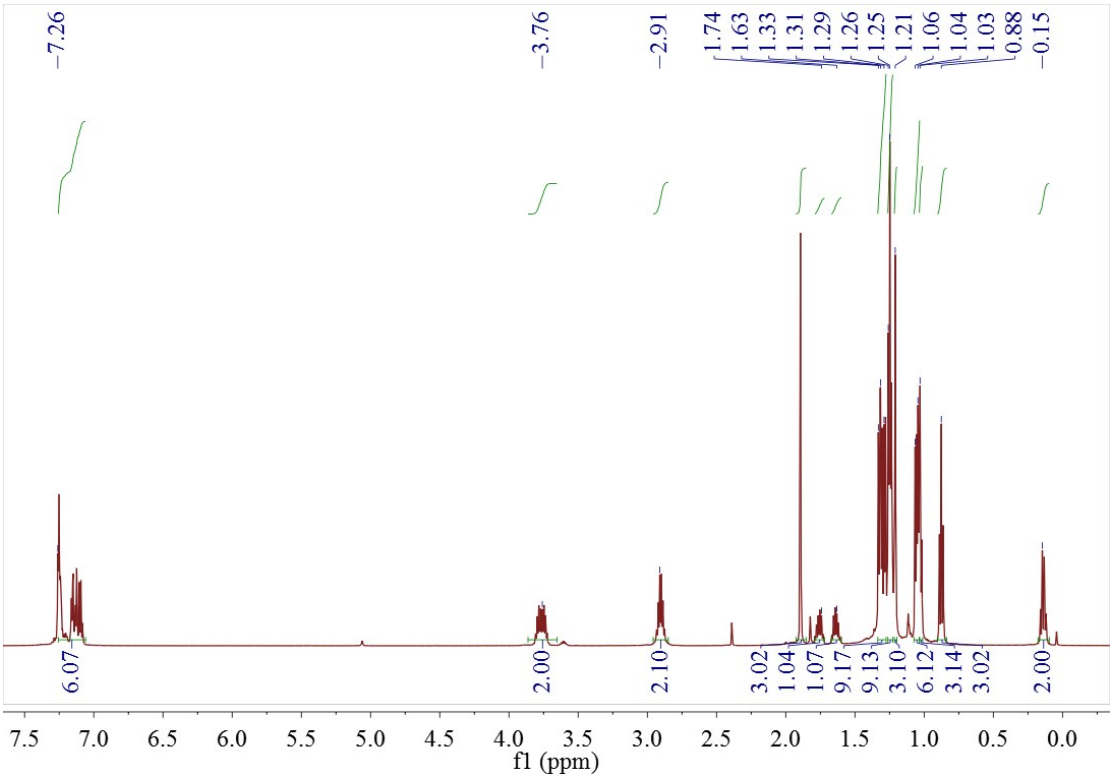

Figure S23. ^{1}H NMR (400 MHz $CDCl_3$ 298K) spectrum for compound **6**.

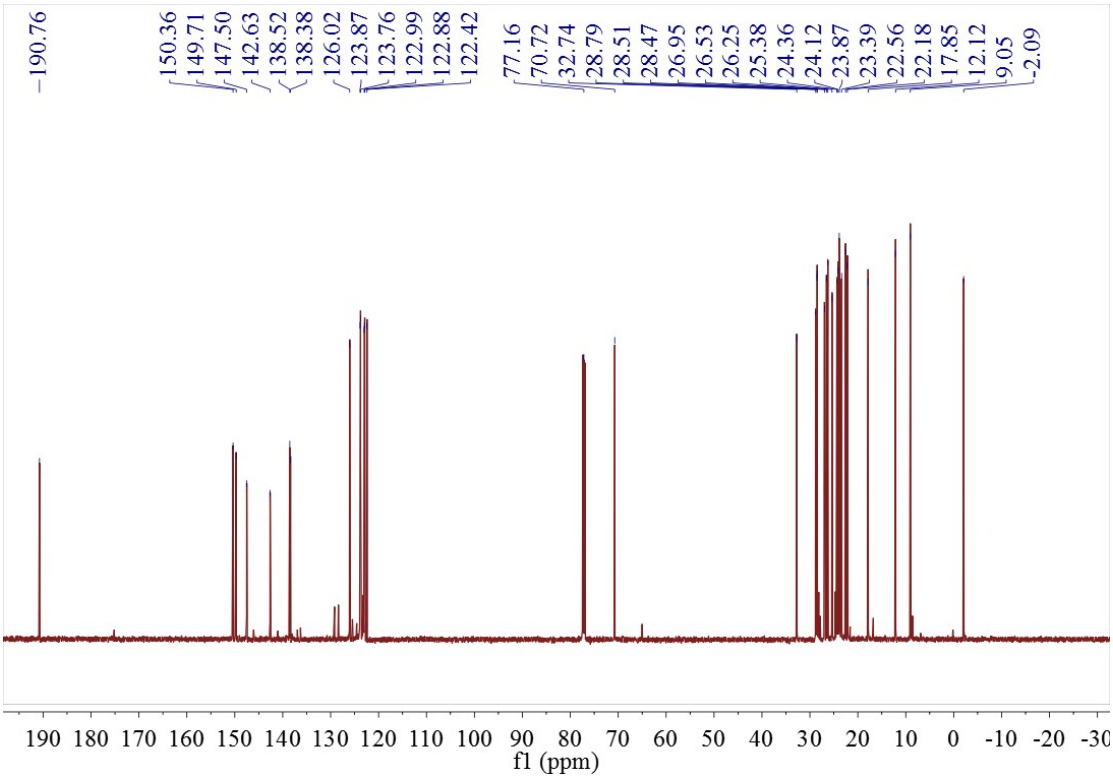

Figure S24. ^{13}C NMR (100.6 MHz $CDCl_3$ 298K) spectrum for compound **6**.

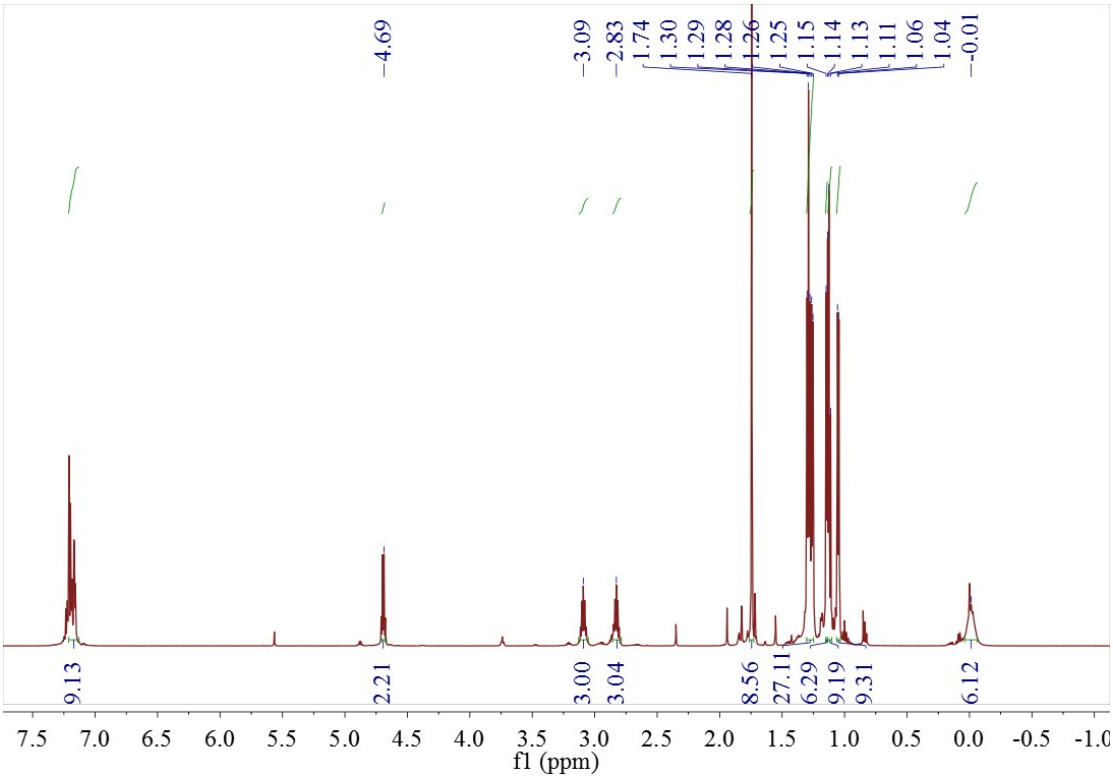

Figure S25. ^{1}H NMR (400 MHz $CDCl_3$ 298K) spectrum for compound **7**.

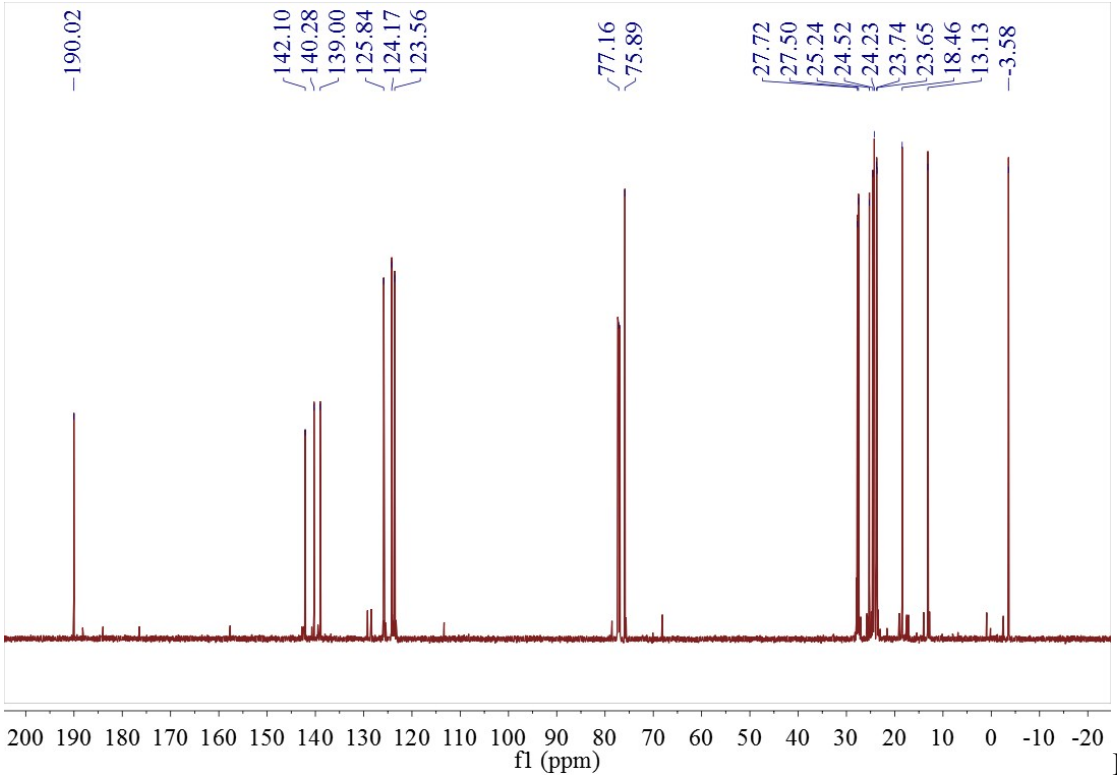

Figure S26. ^{13}C NMR (100.6 MHz $CDCl_3$ 298K) spectrum for compound **7**.

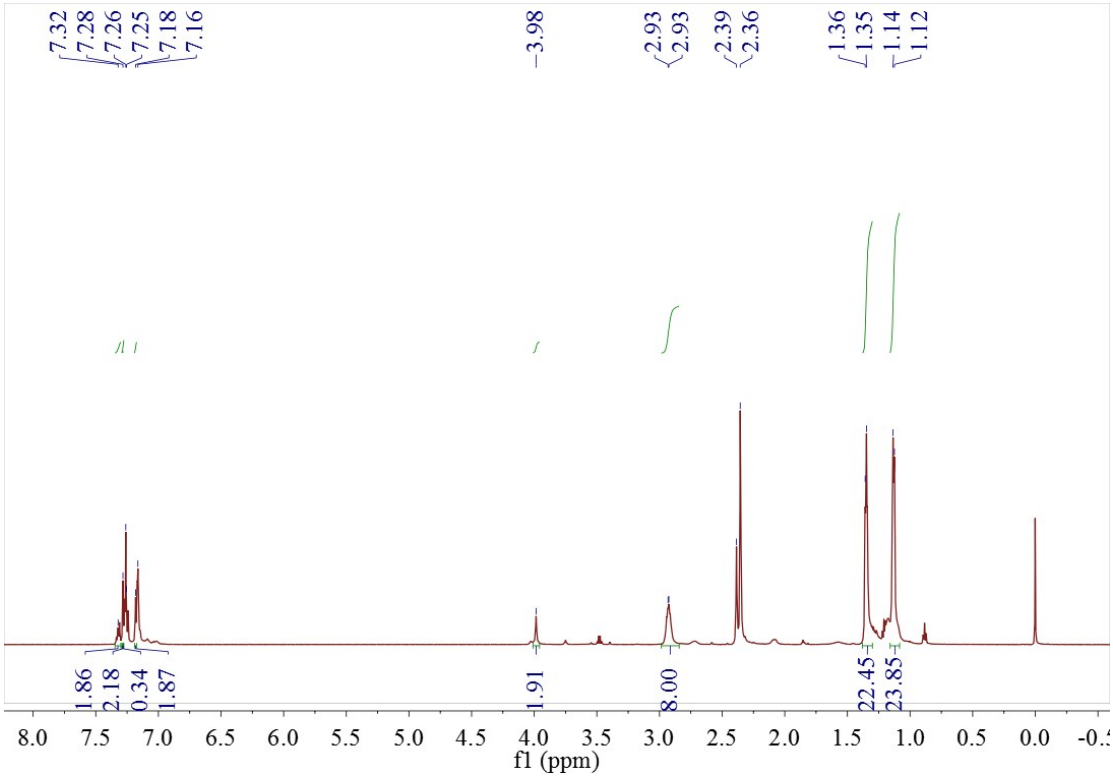

Figure S27. ^{13}H NMR (400 MHz $CDCl_3$ 298K) spectrum for compound **8**.

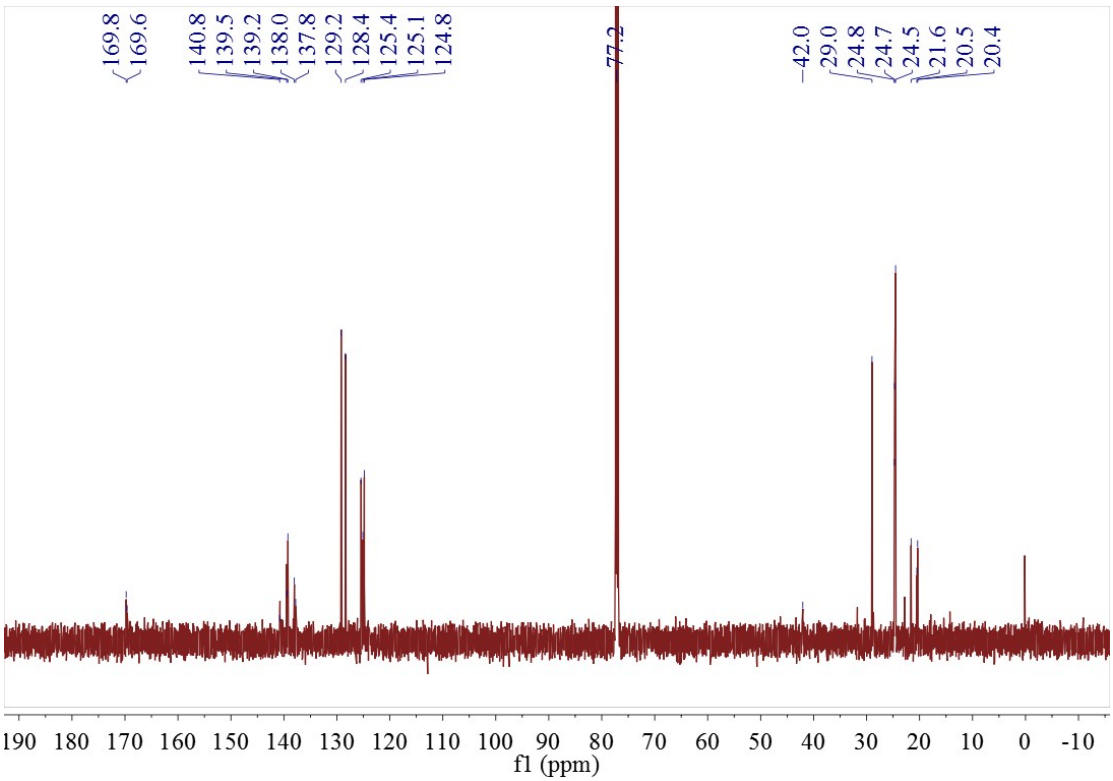

Figure S28. ^{13}C NMR (100.6 MHz $CDCl_3$ 298K) spectrum for compound **8**.

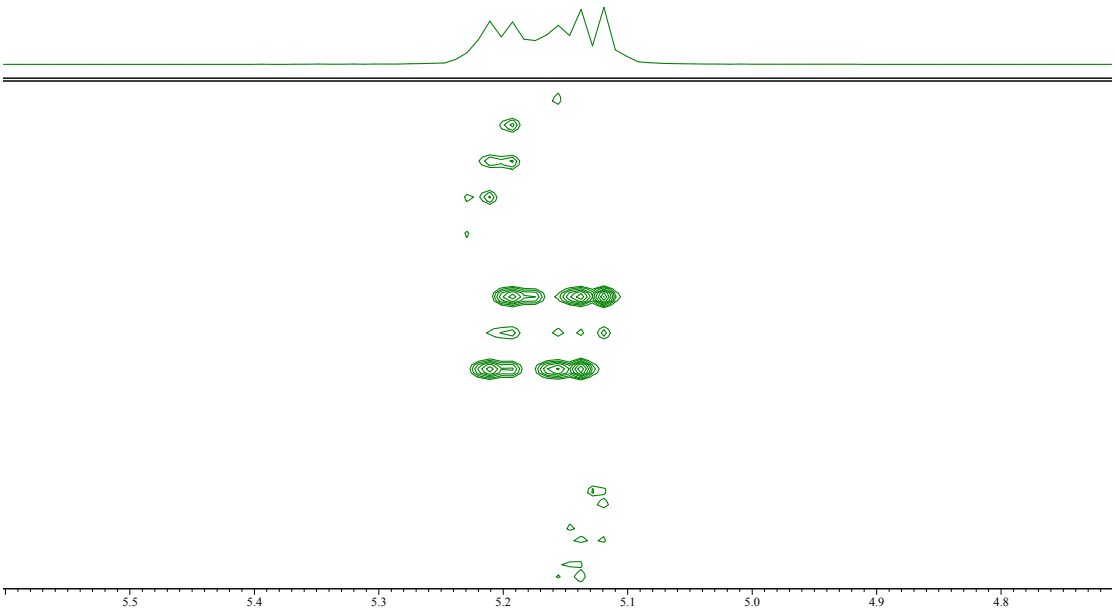

Figure S29. 2D J-resolved ^{1}H NMR ($CDCl_3$, 400 MHz, 298 K) spectrum of the PLA synthesized with **6** at 80 ºC (table 6, entry 2).

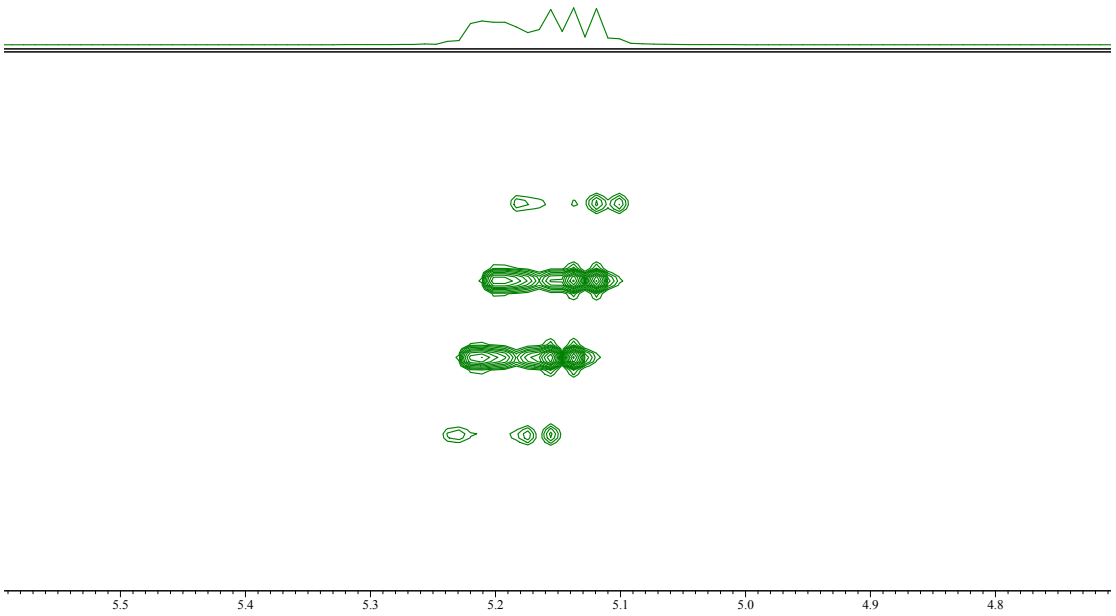

Figure S30. 2D J-resolved ^{1}H NMR ($CDCl_3$, 400 MHz, 298 K) spectrum of the PLA synthesized with **7** at 30 ºC (table 6, entry 3).

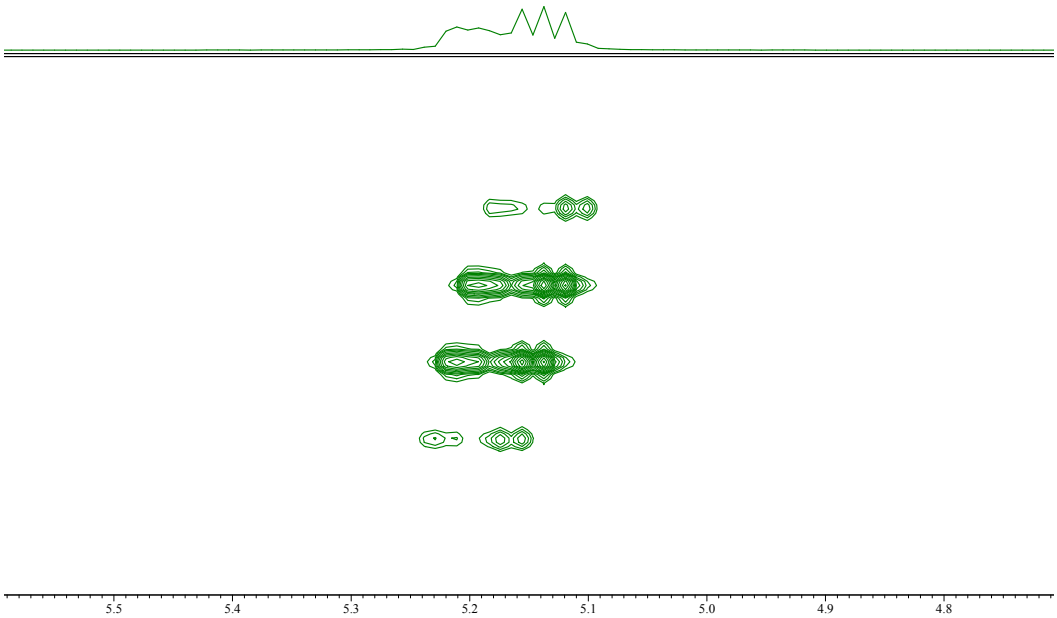

Figure S31. 2D J-resolved ^{1}H NMR ($CDCl_3$, 400 MHz, 298 K) spectrum of the PLA synthesized with **7** at 80 ºC (table 6, entry 4).

References

[1] (a) H. -K. Luo and H. Schumann, *J. Mol. Cat. A: Chem*. 2005, **227**, 153–161; (b) S. Jie, D. Zhang, T. Zhang, W. -H. Sun, J. Chen, Q. Ren, D. Liu, G. Zheng and W. Chen, *J. Organomet. Chem*. 2005, **690**, 1739–1749; (c) J. D. A. Pelletier, J. Fawcett, K. Singh and G. A. Solan, *J. Organomet. Chem*. 2008, **693**, 2723–2731; (d) S. Kong, K. Song, T. Liang, C. -Y. Guo, W. -H. Sun and C. Redshaw, *Dalton Trans*. 2013, **42**, 9176–9187; (e) L. Zhu, Z. -S. Fu, H. -J. Pan, W. Feng, C. Chen and Z. -Q. Fan, *Dalton Trans*. 2014, **43**, 2900–2906; (f) Q. Xing, K. Song, T. Liang, Q. Liu, W. -H. Sun and C. Redshaw, *Dalton Trans*. 2014, **43**, 7830–7837.

[2] A. D. Becke, *J. Chem. Phys.*, 1993, **98**, 5648–5652.

[3] C. Lee, W. Yang and R. G. Parr, *Phys. Rev. B.*, 1988, **37**, 785–789.

[4] Gaussian 09, Revision C.1, M. J. Frisch, G. W. Trucks, H. B. Schlegel, G. E. Scuseria, M. A. Robb, J. R. Cheeseman, G. Scalmani, V. Barone, B. Mennucci, G. A. Petersson, H. Nakatsuji, M. Caricato, X. Li, H. P. Hratchian, A. F. Izmaylov, J. Bloino, G. Zheng, J. L. Sonnenberg, M. Hada, M. Ehara,; K. Toyota, R. Fukuda, J. Hasegawa, M. Ishida, T. Nakajima, Y. Honda, O. Kitao, H. Nakai, T. Vreven, Jr., J. A. Montgomery, J. E. Peralta, F. Ogliaro, M. Bearpark, J. J. Heyd, E. Brothers, K. N. Kudin, V. N. Staroverov, R. Kobayashi, J. Normand, K. Raghavachari, A. Rendell, J. C. Burant, S. S. Iyengar, J. Tomasi, M. Cossi, N. Rega, J. M. Millam, M. Klene, J. E. Knox, J. B. Cross, V. Bakken, C. Adamo, J. Jaramillo, R. Gomperts, R. E. Stratmann, O. Yazyev, A. J. Austin, R. Cammi, C. Pomelli, J. W. Ochterski, R. L. Martin, K. Morokuma, V. G. Zakrzewski, G. A. Voth, P. Salvador, J. J. Dannenberg, S. Dapprich, A. D. Daniels, Ö. Farkas, J. B. Foresman, J. V. Ortiz, J. Cioslowski and D. J. Fox, Gaussian, Inc., Wallingford CT, 2009.